Journal of Remote Sensing & GIS

Classification and Mapping of Land Cover Types and Attributes in Al-Ahsaa Oasis, Eastern Region, Saudi Arabia Using Landsat-7 Data

Abdelrahim Salih[*]

Department of Geography, Al-Imam Muhammad Ibn Saud Islamic University, Al-Ahsaa, Saudi Arabia

[*]**Corresponding author:** Abdelrahim Salih, Department of Geography, Al-Imam Muhammad Ibn Saud Islamic University, Al-Ahsaa, Saudi Arabia, Tel: +966538802619;
E-mail: aSalih@imamu.edu.sa

Abstract

Information about land use/cover is important and much more needed for different aspects of sustainable development and environmental management. Remote sensing datasets has become one of the most important and convenient tool to provide such information. The present study aimed to map land cover types for sub area in Al-Ahasaa Oasis, Saudi Arabia, using a subset of Landsat-ETM+ image. Different image preprocessing techniques in addition to a well-known and widely used classification method (i.e., Maximum Likelihood classifier) were applied. Accuracy assessment was carried out with 89% agreement and accepted according to the applied method. A different land cover classes were found in the study area, which includes (Sand dunes, Water bodies, Sabakha, Bare soil, Urban, and Agricultural lands). The study also revealed that the dominant land cover class is sand dunes with area approximately ± 70%. The study strongly indicated that the area has long been affected by sand movement. Finally, the study suggested that, further researches with more advanced methods rather than traditional methods are needed in the future to support the findings of this study, with a high degree of accuracy.

Keywords: Remote sensing; Classification; Al-Ahsaa; Saudi Arabia; Land cover

Introduction

Knowledge of land use and land cover is important for many planning and management activities concerned with the surface of the earth [1]. Understanding the distribution of land cover is crucial to the better understanding of the earth's fundamental characteristics and processes, including productivity of the land, the diversity of plant and animal species, and the biogeochemical and hydrological cycles [2]. The availability and accessibility of accurate and timely land cover information play an important role in many global land development, and in many scientific studies and socioeconomic assessments because they are essential inputs for environmental and ecological models [3], the primary reference for ecosystem control and management [4] and required information for understanding coupled human and natural system [5].

The need for accurate and up to date information about land cover types [6,7] are necessary and required at different spatial and temporal scales for the purpose of development.

In the study area, little information and a few studies about the land use/cover types have been found. The only study conducted by Aldakheel et al. [8] has been conducted in the study area, have pointed that the use of multi-temporal Landsat TM imagery to detect land use/cover change showed a significant result. They also reported that vegetation, soil salinization and urban area are the dominant land cover types in the study area.

However, accurate and up to date information about land cover types and attributes is much more needed, and the available information needs further investigation.

The use of Landsat image to map land use and land cover has been an accepted practice since the launch of Landsat-1 in 1972. Land cover mapping is one of the main areas of remote sensing data application [9,10].

To effectually obtain such information from remotely sensed data, convenient digital image classification methods are required. A number of classification techniques have been reported for gathering, monitoring and mapping land cover types using remote sensing data [1,6,11-15]. (e.g., Osman [12] suggested the nonparametric methods or knowledge-based for image processing and analysis. Sub pixel classification methods [13,16,17] have been used to label the mixed land cover class especially in arid and semi-arid environment. However, these methods would not be suitable within the limited resource and because it requires limited and spectrally distinctive components. In addition to, the remotely sensed signal of a pixel should linearly relate to the fraction of endmember present [16]. Conventional methods have also been widely accepted and used for mapping and assessment of land use and land cover types from satellite image [1,12,18].

In the present study, classification and mapping of land cover types from Landsat-7 (ETM+) image is the main objective. In addition, identification of land cover attributes is second focus. Level 1 of the USGS [19] classification system is applied using the standard supervised (i.e., Maximum Likelihood) classification method, aided by different image preprocessing techniques. More details about the study area and materials and research methods are described in section materials and methods of the paper. In results section, more information about research results are presented. Finally, the study discusses the main points and findings of the subject of the paper in discussion section and draw general conclusions in conclusion section.

Materials and Methods

Study area

The study taken place in Al-Ahsaa Oasis, eastern region, Saudi Arabia. It covers approximately 2268.72 km^2 in area, with the geographical coordinates (49°24'-49°48' E and 25°24'-25°36' N), (Figure 1). The study area is mainly covered by active sand dunes. The topography as shown in Figures 2a and 2b is very gentle with little relief and a few surrounding ridges. The elevation ranges from 345 to 510 meters above sea level. The study area is affected by arid and semi-arid climate, with average annual rainfall less than 46 mm, and mean annual temperature is approximately 28°C in summer. The peak rain falls almost entirely in the period of March and August.
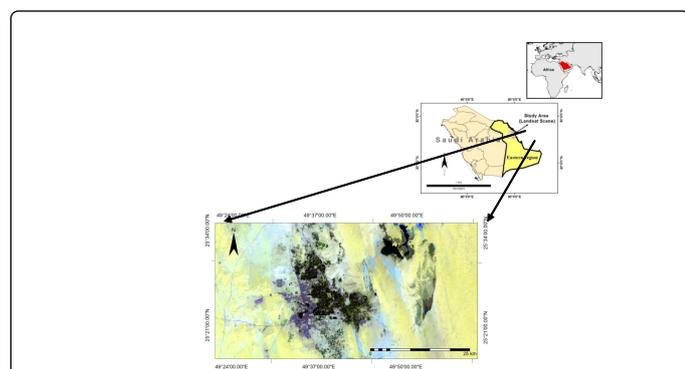
Figure 1: Location of the study area in Al-Ahsaa, Eastern Region of Saudi Arabiya. The image from Landsat-7 ETM+ channel 7,5,1.
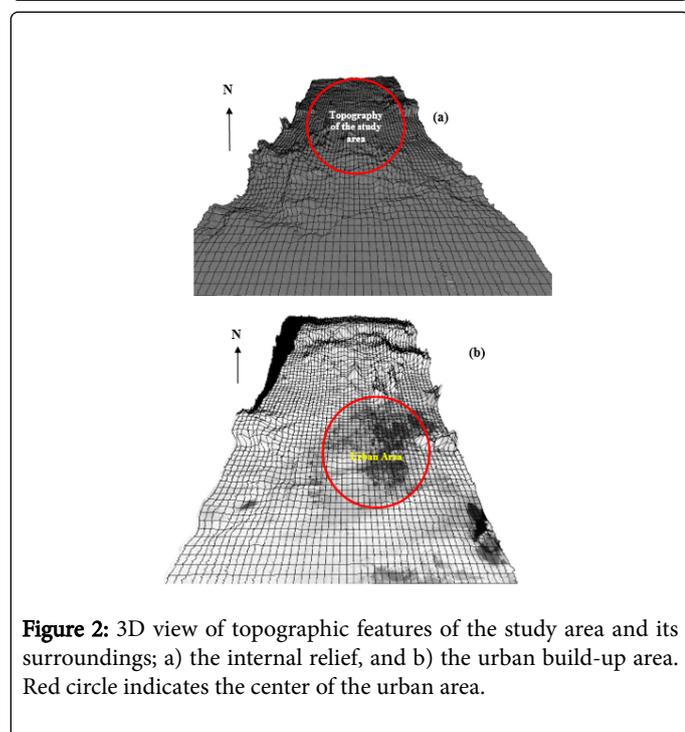
Figure 2: 3D view of topographic features of the study area and its surroundings; a) the internal relief, and b) the urban build-up area. Red circle indicates the center of the urban area.

For generating the land cover map, several and essential image pre-processing and analysis techniques were used. All the image processing and analyses have been carried out by using an Integrated Land and Water Information system (ILWIS) open source software. ILWIS is software with Geographical Information System (GIS) and Image Processing capabilities.

Image pre-processing

For several reasons, raw remotely-sensed data generally contain geometric and radiometric errors [20]. To classify, identify and extract spectral and spatial classes representing different thematic features of these data [21], these errors have to be removed or eliminated. In this study, the geometric corrections were already done by the data provider, while the necessary radiometric corrections were accomplished as previously described in Irish and Mather [18,20].

Image classification

There is a relationship between land cover and measured reflection values in the image data, which depends on the local characteristics [22]. In order to extract information from the image data, this relationship must be found. The process to find this relationship is called classification. Digital image classification is customarily made by applying either supervised or unsupervised classification methods [1,12]. For satellite image applications, the latter is generally considered much more important and widely used [22]. In this study, the supervised classification method was applied to classify sub-scene of the Landsat-7 ETM+ image. In the following steps, the classification procedures were given:

- By using three uncorrelated bands (7, 5, and 1) have been obtained from the optimum index factor (O.I.F), a false colour composite image was created.
- Three image transformation methods were used. These are: a) Principal Components Analysis (PCA) was used as enhancement to reduce and remove data dimensionality and redundancy (Liu and Mason, 2009) prior to visual interpretation classification of the original data, b) Image subtraction (differencing) was used for spectral enhancement and removal of background illumination bias(Mather 1987):, c) Image division (ratio) was used to enhance spectral features, and finally d) Normalized Difference Vegetation Index (NDVI) was used for detection vegetation spectral response.
- By using data derived from step 1 and 2, two sets of signature files were defined and collected aided by the groups of "ground truth points".
- For signatures evaluation, the created signature files were plotted in colors feature space (see Figure 3), to confirm and judgment that, the selected land cover classes are spectrally distinguished, and each class corresponds to only one spectral cluster [22], (i.e., no obvious overlap exist) between different features.
- By using the signature files generated in step three, the supervised classification (maximum likelihood algorithm) was applied in a semi-automatic way and the obtained result was evaluated and tested for accuracy.
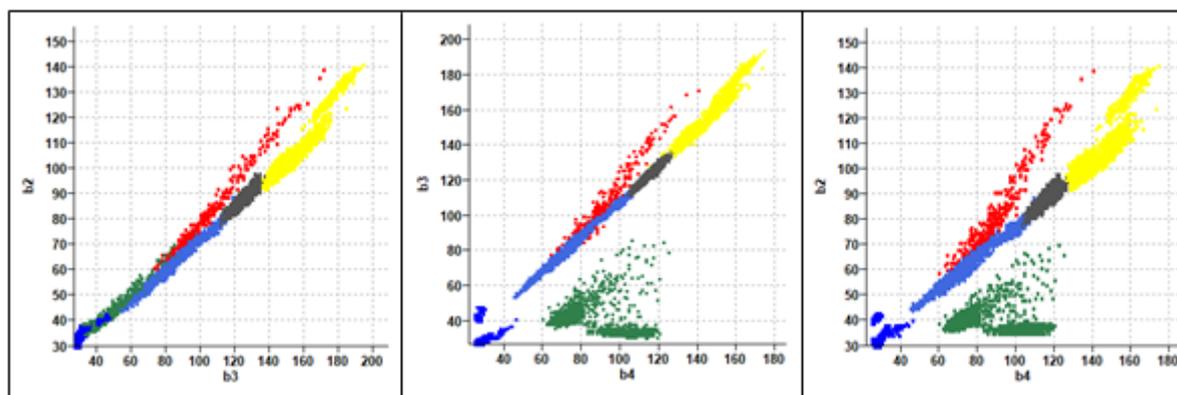
Figure 3: Overlap of the features space of the training areas; a) band 4 and band 2; b) band 4 and band 3; and c) band 3 and band 2.

Results

Image transformation results

The six original bands 1-5 and 7 (Band 6, is a thermal band, it makes TM data potentially useful in a range of thermal mapping applications. Also, band 6 has a less distinct appearance than the other bands because of the ground resolution cell of this band is 120 m. Therefore, it was excluded from band combination and preprocessing and analysis) of the Landsat-7 ETM+ image are highly correlated with one another. To compact the redundant data into fewer layers, PCA was used to produces a new set of image, that are uncorrelated with one another and are ordered in terms of the amount of variance they explain from the original set of bands. The eigenvector matrix of six reflective spectral bands of subset of a Landsat ETM+ image is presented in Table 1. The six PC components derived from original image are shown in Figure 4. The following observations are made:

- The eigenvalues representing the variances of PCs shown in Table 1 indicates that a very large portion of information (data variance) is concentrated in PC1 and PC2 with 98.92% of the total variation in the original data set. Whereas, the others PC (i.e., PC3, PC4, PC5, and PC6) together account for only about 1.08% of the total variance in the original scene. Also from Table 1 it can be seen that all the bands had a positive eigenvectors (weight) in PC1. According to Olmo et al., Singh et al. and ILWIS [22-24] these eigenvectors are interpreted as: a) albedo image (in which the soil and sand background is represented), b) mostly explains the high difference of the input bands.

- From Table 1 and Figure 4 note that PC1 highly concentrates approximately (94.35 percent) of the variance in the original data.

- All six bands have positive contribution with large eigenvalue (5007.30 variance) and accounts for more than 94% of the information from all six bands. From eigenvectors in row 1 note that large positive loading (0.655) from band 5 and (0.454) from band 7 caused by the high reflectance of sand dunes and urban areas.

- The PC images with small eigenvalues (variance) (e.g., PC5 and PC6) contain no information. It is almost no more than errors or noise.

- By referencing to Figure 4, PC1 concentrates information common for all six bands. According to the visual interpretation, this common information is mostly sand dunes.

- From Figure 4, both PC2 and PC3 depict the largest amount of variance that was inconspicuous by the dominant information of PC1. For instance, some urban areas, natural vegetation and sand sheet are obviously defined in the PC2 and PC3 with bright and grey colour.

- Row 2 of Table 1 illustrates the eigenvectors values of PC2 that is dominated by the contribution of the blue band (channel 1) with large positive loading (0.753) and large negative loading (-0.453) from mid-infrared band (channel 7). The large loading of PC2 is mostly representing the information excluded from PC1. PC3 and PC4 are dominated by large positive loading (0.437) and (0.682) from mid-infrared (channels 5 and 7). The large positive loading of PC3 as shown in Figure 4 is caused by the higher reflectance of urban areas and vegetation given by mid-infrared band (channel 7), whereas the large positive loading of PC4 is because of noise.

- As the PCA operation made the bands independent or orthogonal from one another, bands with high amount of information (high variance) (i.e., PC1, PC2, and PC3) are used to create a colour composite image as shown in Figure 4. From the created image, definition and collection of training areas were easily achieved with less overlap as plotted in Figure 3.

From Table 1 the too many positive eigenvectors value in band 1 could be justified by the following:

- The study area is dominated by sand cover, bare soil, and the availability of Sabakha's feature. These features are highly reflected by band 1 where this band is designed for discrimination of soil and vegetation and cultural feature identification.

- Band 1 is highly correlated with band 2(0.96%), 3(0.90%) and 4 (0.84%) and less correlated with band 5 and 7 (largest sum of standard deviation between this two bands is 46.62, and 33.09) and smallest correlation. It can justify that, band 1 to 3 having similar information with high concentration in band1.

Figures 4 and 5 shows the image transformation results. The results highlighted the cover feature classes in the image by enhancing spectral features separability and suppressing topographic shadows.

|	band1	band2	band3	band4	band5	band7
PC 1	0.276	0.231	0.39	0.289	0.655	0.454
PC 2	0.753	0.299	0.232	0.074	-0.279	-0.453
PC 3	0.289	0.076	-0.005	-0.845	-0.077	0.437
PC 4	0.18	-0.185	-0.396	-0.268	0.682	-0.489
PC 5	0.431	-0.164	-0.696	0.354	-0.14	0.396
PC 6	0.232	-0.889	0.39	0.017	-0.046	0.032

Table 1: The PCA eigenvalues (variance) and eigenvectors of the covariance matrix of Landsat-7 ETM+ sub-scene. Variance per bands: 5007.30, 242.67, 31.08, 41.46, 10.38, 1.06. Variance percentage per band: 94.35, 4.57, 0.59, 0.27, 0.20, 0.02.
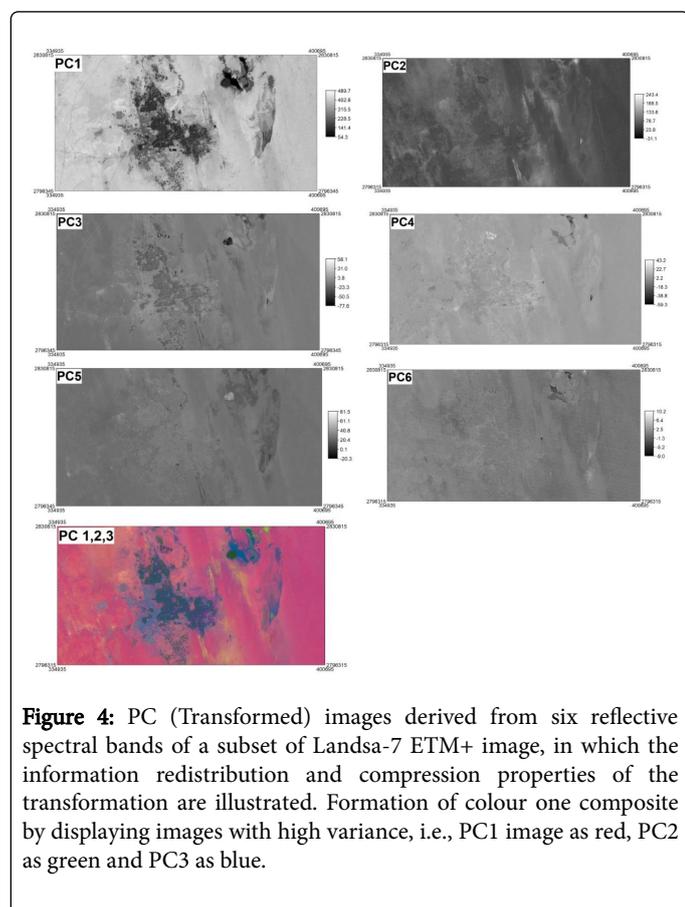

Figure 4: PC (Transformed) images derived from six reflective spectral bands of a subset of Landsa-7 ETM+ image, in which the information redistribution and compression properties of the transformation are illustrated. Formation of colour one composite by displaying images with high variance, i.e., PC1 image as red, PC2 as green and PC3 as blue.

From Figures 4 and 5, it can be seen that the areas covered by sand and barren lands or bare soil were easily distinguished and sampled. The concentrations of Iron oxides and hydroxides in minerals, made the spectral reflectance of sand (represented by the pink colour in Figure 5 and by red colour in Figure 6 more apparent in the resulting images than the original one. The urban (Built-up) areas are more apparent in Figure 6 than in Figure 5, that indicated by blue colour. Therefore, it was easily sampled and classified. Agricultural areas are indicated by green colour in Figure 5 and turquoise colour in Figure 6 due to higher moisture content of this cover type. The Sabakha's feature is indicated and highlighted by brown colour as shown in Figure 5.

However, image transformation (i.e., PCs and image ratios) techniques are very useful and valuable for highlighting and distinguishing specific land cover classes spectrally rather than spatially. Therefore, it is usage was restricted just to define and collect the training samples for classification purpose.
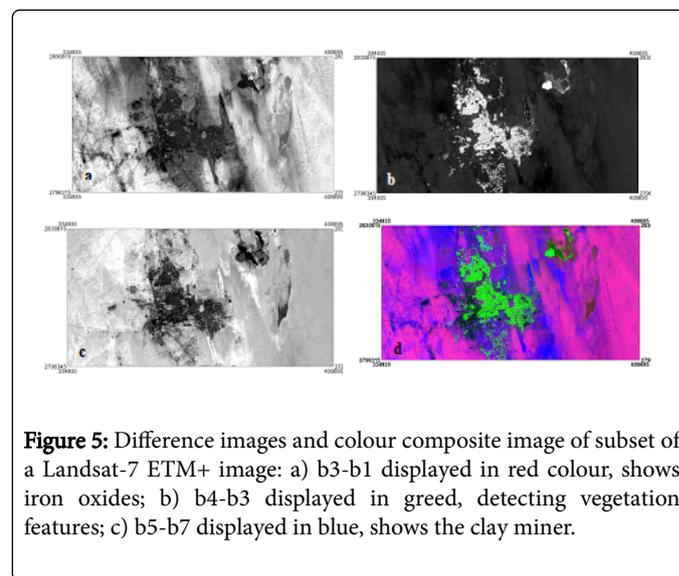
Figure 5: Difference images and colour composite image of subset of a Landsat-7 ETM+ image: a) b3-b1 displayed in red colour, shows iron oxides; b) b4-b3 displayed in greed, detecting vegetation features; c) b5-b7 displayed in blue, shows the clay miner.
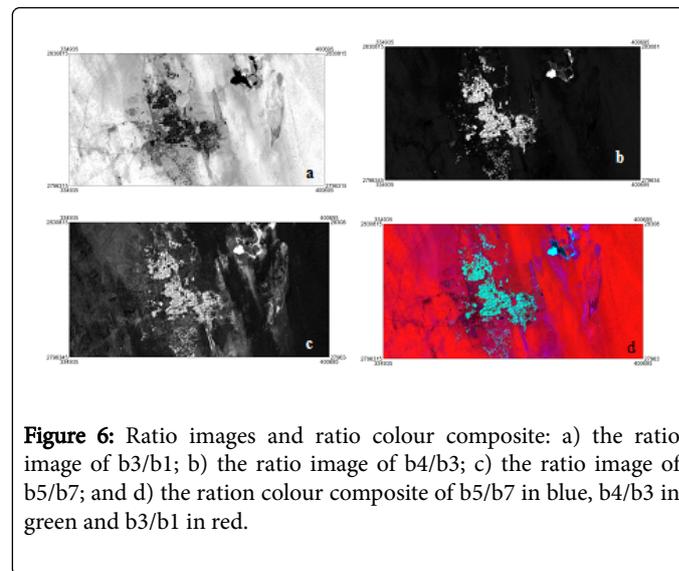

Figure 6: Ratio images and ratio colour composite: a) the ratio image of b3/b1; b) the ratio image of b4/b3; c) the ratio image of b5/b7; and d) the ration colour composite of b5/b7 in blue, b4/b3 in green and b3/b1 in red.

Figure 7 shows the healthy vegetation cover in the study area as difference and summation of the Near Infrared (NIR) and red spectrally calibrated bands (i.e., NDVI) index. This index was applied to make vegetation cover more distinguishable from the other ground objects for better classification results. The derived NDVI values ranging from -0.30 as a minimum NDVI value representing the area covered by water body, to 0.60 as maximum NDVI value, representing the area covered by vegetation.
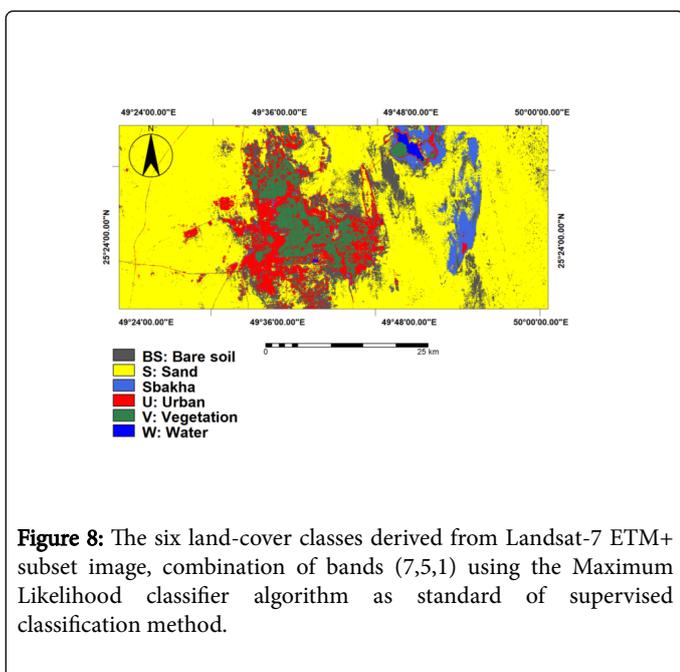
Image classification results

Figure 8 shows the result obtained from classified subset Landsat-ETM+ image. Six major land cover classes have been found in the study area, namely: (Vegetation (Agriculture), Sabakha, Sand, Bare soil, Water body, and Urban).
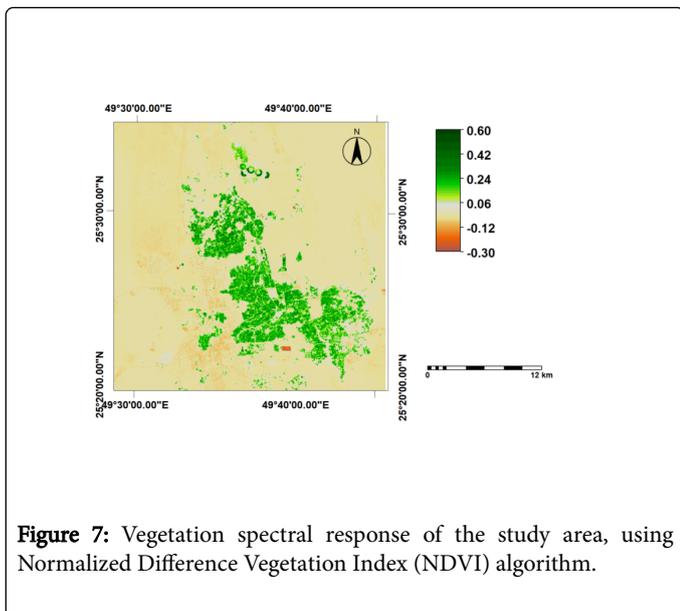
Figure 7: Vegetation spectral response of the study area, using Normalized Difference Vegetation Index (NDVI) algorithm.

Information about areal and percentage of thematic classes are summarized and presented in Table 2. By referencing to Table 2, the sand dune class is dominant in the study area, it covers about 70% of the study area. The absence of vegetation cover on the study area sides is conspicuous. There is, however, a few vegetation cover near water bodies in the form of bushes. Figure 8 also shows that the agricultural areas are only cover 5% in the area, mainly date trees with a few vegetables around it. Urban areas cover approximately 8% of the study area. According to the urban shape and pattern, it is clear that the urban growth and extension of the study area is in the North-South and East direction. This meant that the extension of the urban is restricted by different factors (e.g., Sand dunes).

Figure 8: The six land-cover classes derived from Landsat-7 ETM+ subset image, combination of bands (7,5,1) using the Maximum Likelihood classifier algorithm as standard of supervised classification method.

Accuracy assessment

Table 3 shows the statistical report of the cross function that was used to evaluate the accuracy of the classification result, using the second set of signature file. The overall accuracy is 79%, with average accuracy 89% and average reliability 83%, which demonstrate that the good performance of classification procedures. Generally speaking, statistical information from Table 3 indicates that the error of accuracy and reliability is less than 17 percent. By referencing to the accuracy and reliability statistical information, the classification results are accepted as basis for better planning and management of the existing land resources in the study area.

Class	N pixels	Area (meter)	Area (km^2)	Area (%)
Bare soil	289886	260897400	260.8974	11.5
Sand	1768623	1591760700	1591.7607	70.16
Sbakha	88953	80057700	80.0577	3.53
Urban	219415	197473500	197.4735	8.7
Vegetation	145937	131343300	131.3433	5.79
Water	7986	7187400	7.1874	0.32
Sum	2520800	2268720000	2268.72	100

Table 2: Major land-cover classes found in the area in (Meter, Km^2 and percentage) created by the classification of Landsat-7 ETM+ subset image (channel 1,5,7).

Discussion

A study of Landsat-ETM+ image of the study area reveals that a large variety of sand dune shapes were found. With a total area estimated at 1591 square kilometer, has a sand cover. At least one-third of the study area has been affected by sand movement. The problem of sand movement has been controlled for several years by planting different types of trees utilized to control and stabilize the sand movement toward the urban built-up area. Different shapes and sizes of sand dunes have been found in the study area. Holm [25] pointed out that the main sources for these sand dunes are: the Rub' al Khali, Nafud's, and Dahna deserts. He also reported that the primary sources of sand for these deserts are crystalline rocks exposed in the uplands of the peninsula. An observation from field work suggests that most of the sand dunes occur in areas of low relief, and low plains, as shown in the East and West of the study area. In the Eastern part of the study area, the dunes high are about ± 150 meters. The second more interesting cover type has been found in the study area is Sabakha's features (indicated by blue colour in the land cover map). A study by Holm [25] pointed out that the name is from the Arabic, and the sabakha is a saline flat area, and are found inland from the coast at elevations up to 150 meters near Hofuf (The focus of this study). Most of this type of land cover has long been concentrated in the Eastern part of the study area (see Figure 8). Also Holm [25] reported that there are two types of sabakha's formation along the Arabian coast, these are: 1) arenaceous, filled with sand, and 2) aregillaceous, filled with clay.

	Bare soil	Sand	Sabakha	Urban	Vegetation (Agriculture)	Water	Unclassified	Accuracy
Bare soil	1	0	0	0	0	0	0	1
Sand	1	1107	0	0	0	0	0	1
Sabakha	1456	0	869	4	0	0	0	0.37
Urban	1	0	0	459	0	10	0	0.97
Vegetation	0	0	0	1	1364	2	0	1
water	0	0	0	0	0	1771	0	1
Reliability	0	1	1.99	0.99	1	0.99		

Table 3: Classification accuracy assessment results of Landsat-7 ETM+ subset image, Date: October 2017, bands combination (1,5,7). Average Accuracy=89.08%; Average Reliability=83.03%; Overall Accuracy=79.05%.

For more details and more information about the formation of this land cover type, the study has been carried out by Holm [25] can be considered and suggested. Also from Table 2, can be seen that the agricultural areas only cover around 131 square kilometer (i.e., approximately 5%) from the whole study site. One may interpret that for some reasons; the first reason is that the study area has long been affected by different kinds of drought (e.g., hydrological droughts), the second reason is that the study area has been experiencing steady growth in its population since 2000 up to now. From 2000 until today, the built-up areas are increased to reach approximately ± 197 km^2 in area in 2017. In addition to that, the extension of built-up area has recently restricted by sand dune to be extended in specific directions (i.e., toward the agricultural lands). All these factors lead to decrease the areas covered by crop land in the study area. Different land use/cover classes have been found by Aldakheel and Al-Hussaini [8]. They also revealed that channel 3 of Landsat TM image may best used to discriminate conversion land of rural to urban among the land cover classes in change detection method. However, what they have been found and what has been found in this study, needed more investigation and in deep research using more ground truth and different methods of remotely sensed data analysis (e.g., Object-based classification, decision trees and support vector machines) than traditional methods (i.e., supervised or unsupervised) to better findings and generalizing the findings for the whole region and generating more accurate and reliable land use/cover map.

Conclusions

The aim of this study was to generate up-to-date land-cover map of the Al-Hofuf study site based on a well-known and widely applied (i.e., maximum likelihood classifier algorithm) standard supervised classification method using Landsat-7 ETM+ subset image data. From the obtained results, the study concludes that:

Results from the study revealed that using image transformations prior to image classification decreased the topographical effects (i.e., shadows) on the satellite image and make it more consistence for classification application, and more appropriate for the definition and collection of training areas, especially for (urban and sabakha). It is also concluded that the correlation matrix (i.e., O.I.F) was very useful to obtain multivariate statistical information of a data set for 3-band combination.

By referencing to the applied methods and overall accuracy results, the generated land-cover map may considered for land resources management and development. Furthermore, the study concludes that Landsat-ETM+ image data give optimal and up-to-date information regarding land use/cover mapping, and very useful to carry out land use/cover studies in wide arid and semi-arid area.

Finally, the results also pointed out that the study area has long been affected by sand movement. Therefore, more studies in the future should take place in the study area for more information about this phenomenon (i.e., Sand Encroachment).

Acknowledgments

Author Contributions

All the work of the paper has been carried out by the author.

Conflicts of Interest

The authors declare no conflict of interest.

References

1. Lillesand TM, Kiefer RW (1989) Remote Sensing and Image Interpretation. John Wiley & Sons Ltd, London, UK, p: 721.

2. Giri CP (2012) Remote Sensing of Land Use and land Cover: Principles and Applications. Series in Remote Sensing Applications. Taylor & Francis, UK.

3. Bontemps S, Herold M, Kooistra L, Van Groenestijn A, Hartely A, et al. (2012) Revisiting land cover observation to address the needs of the climate modeling community. Biogeosciences 9: 2145-2157.

4. Yang J, Gong O, Fu R, Zhang M, Chen J, et al. (2013) The role of satellite remote sensing in climate change studies. Nat Clim Chang 3: 875-883.

5. Mora B, Tesndbazar NE, Herold M, Arino O (2014) Global land cover mapping: Current status and future trend. In: Land cover change detection by integrating object-based data blending model of Landsat and MODIS. Remote Sensing of Environment 184: 374-386.

6. Chen J, Chen J, Liao A, Cao X, Chen L, et al. (2015) Global land cover mapping at 30 m resolution: A POK-based operational approach. ISPRS J Photogramm Remote Sens 103: 7-27.

7. Jin S, Yang L, Danielson P, Homer C, Fry J, et al. (2013) A comprehensive change detection method for updating the National Land cover Database to circa 2011. Remote Sens Environ 132: 159-175.

8. Aldakheel Y, Al-Hussaini A (2005) The use of multi-temporal Landsat TM imagery to detect land cover/use changes in Al-Ahssa, Saudi Arabia. Scientific Journal of King Faisal University (Basic and Applied Sciences) 6: 1426.

9. King RB (2002) Land cover mapping principles: a return to interpretation fundamentals. International Journal of Remote Sensing data, Remote Sensing of the Environment 86: 530-541.

10. Foody GM (2002) Status of land covers classification accuracy assessment. Remote Sensing of the Environment 80: 185-201.

11. Pilesjö P (1992) GIS and Remote Sensing for Soil Erosion Studies in Semi-arid Environment: Estimation of Soil Erosion Parameters at Different Scales. Doctor's thesis No. CXIV, Department of Physical Geography, University of Lund, Sweden, p: 203.

12. Osman BT (1996) GIS-Hydrological Modelling in Arid Lands: A geographical synthesis of surface waters for the African Red Sea region in the Sudan. Doctor's thesis, Department of Physical Geography, University of Lund, Sweden, p: 202.

13. Salih AAM, Ganawa E, Elmahl AA (2017) Spectral mixture analysis (SMA) and change vector analysis (CVA) methods for monitoring and mapping land degradation/desertification in arid and semi-arid area (Sudan), using Landsat imagery. The Egyptian Journal of Remote Sensing and Space Sciences 20: 21-29.

14. Sobrino JA, Munoz JCJ, Paolini L (2004) Land surface temperature retrieval from LANDSAT TM5. Remote Sensing of Environment 90: 434-440.

15. Erener A, Düzgün S, Yalciner AC (2011) Evaluating land use/cover change with temporal satellite data and information system. Procedia Technology 1: 385-389.

16. Song C (2005) Spectral mixture analysis for sub-pixel vegetation fraction in the urban environment: How to incorporate endmember variability. Remote Sensing of Environment 95: 248-263.

17. Dawelbait M, Morari F (2012) Monitoring desertification in a Savannah region in Sudan using Landsat images and spectral mixture analysis. Journal of Arid Environment 80: 45-55.

18. Irish R (2002) Landsat 7 Science Data Users Handbook. NASA Goddard Spaceflight Centre, USA.

19. US Geological Survey (USGS).

20. Mather PM (2009) Computer Processing of Remotely-Sensed Images: An Introduction. John Wily & Sons Ltd, West Sussex, England.

21. Liu JG, Mason PJ (2009) Essential Image Processing and GIS for Remote Sensing. John Wily & Sons Ltd, West Sussex, UK.

22. ILWIS (2001) User's Guide, Aerospace Survey and Earth Sciences (ITC). Enschede, The Netherlands.

23. Olmo MC, Hernandez FA (2005) Remote Sensing Image Analysis: Including the Spatial Domain, Netherlands, pp: 93-111.

24. Singh A, Harrison A (1985) Standardized Principle Components. International Journal of Remote Sensing 6: 883-896.

25. Holm DA (1960) Desert Geomorphology in the Arabian Peninsula: Distinctive land forms provide new clues to the Pleistocene and Recent history of a desert region. Science 132: 1369-1379.